



# Preparation and application of ordered mesoporous carbon-based solid acid catalysts for transesterification and epoxidation

Lijuan Yang<sup>1</sup> · Hong Yuan<sup>1,2</sup> · Siyu Wang<sup>1</sup>

Published online: 12 March 2019  
© Springer Science+Business Media, LLC, part of Springer Nature 2019

## Abstract

Ordered mesoporous carbon (OMC) was prepared via the inverse replication method using SBA-15 as a hard template and sucrose as a carbon precursor. OMC was sulfonated to obtain the solid acid catalysts, such as OMC-SS and OMC-DS, by heating with sulfuric acid or coupling with sulfanilic acid diazonium. TEM and small-angle X-ray diffraction (XRD) results showed that OMC, OMC-SS, and OMC-DS exhibited ordered porous structures. XPS and Raman analysis showed that OMC had graphite structure. N<sub>2</sub>-BET analysis indicated that OMC, OMC-SS, and OMC-DS had average pore diameters of 3.0–3.3 nm and exhibited bimodal mesopore size distributions. Moreover, N<sub>2</sub>-BET analysis revealed that OMC, OMC-SS, and OMC-DS had surface areas of 1411, 924 and 1001 m<sup>2</sup>/g, respectively. The surface acid contents of OMC-SS and OMC-DS were 3.9–4.0 mmol H<sup>+</sup>/g and higher than those of OCM (2.8 mmol H<sup>+</sup>/g). FTIR results demonstrated that –SO<sub>3</sub>H was present on OMC-SS and OMC-DS. OMC-SS and OMC-DS were used to catalyze the transesterification and epoxidation of waste frying oil. The transesterification reactions catalyzed using OMC-SS and OMC-DS provided the maximum yields of fatty acid methyl esters of 90.3 ± 3.3% and 89.0 ± 2.1%, respectively. The double-bond conversion rates of epoxidation reactions catalyzed using OMC-SS and OMC-DS reached 77.2 ± 1.9% and 68.5 ± 2.6%, respectively. The epoxy yields of epoxidation reactions catalyzed using OMC-SS and OMC-DS were 70.3 ± 2.4% and 65.1 ± 1.8%, respectively.

**Keywords** Ordered mesoporous carbon · Sulfonation · Transesterification · Epoxidation: waste frying oil

## 1 Introduction

Porous carbon materials are widely used in gas separation, water purification, catalysis, photocatalysis, energy storage, and capacitors because of their excellent chemical stabilities and large specific surface areas [1–6]. Conventional porous carbon materials, such as activated carbon and carbon fibers, are uncondusive to the internal pore diffusion of reactants because they possess nonuniform pore sizes and high

micropore contents (< 2 nm). In 2000, Jun et al. first prepared an ordered mesoporous carbon (OMC) material via the reverse replication of SBA-15, which is a two-dimensional (2D) hexagonal mesoporous silica molecular sieve. They used SBA-15 as a template and sucrose as a carbon precursor and designated the product as OMC-3 [7]. In 2001, Joo et al. synthesized OMC-5, an OMC with a tubular structure, using Al-SBA-15 as a template and furfuryl alcohol as a carbon precursor [8]. In 2002, Kaneda et al. prepared OMC-1 and OMC-4 with single-crystal morphology using single-crystal MCM-48 as the template [9]. Since 2001, the research and applications of OMC materials (2–50 nm) have attracted widespread attention. The ordered mesoporous structures of OMC materials favor the mass transfer of reactants by weakening the resistance of internal pore diffusion. At present, OMC materials are widely used in catalysis, hydrogen storage, purification, and sensing [10–13].

Conventional liquid acid catalysts have several shortcomings, such as difficult separation from reactants and environmental pollution generation. Therefore, the study and preparation of suitable solid acid catalysts have become

✉ Hong Yuan  
yuanhong@nun.edu.cn

Lijuan Yang  
1509664518@qq.com

Siyu Wang  
1251330419@qq.com

<sup>1</sup> School of Chemistry and Chemical Engineering, North Minzu University, Yinchuan 750021, China

<sup>2</sup> State Key Laboratory of National Ethnic Affairs Commission Chemical Technology, North Minzu University, Yinchuan 750021, China

popular. Some researchers have attempted to introduce the  $-\text{SO}_3\text{H}$  functional group onto the surfaces of OMC materials to obtain solid acid catalysts. Zhang et al. used SBA-15 as a template, glucose glycerol as a carbon precursor, and concentrated sulfuric acid as a sulfonating agent to synthesize a sulfonated solid acid OMC catalyst. They reported that the conversion rate of the pre-esterification of free fatty acids catalyzed using the sulfonated OMC-based solid acid catalyst reached 94.6% [14]. Eika et al. adopted SBA-15 as a mesoporous silica template, sucrose as a carbon precursor, and concentrated sulfuric acid as a sulfonation reagent to prepare a sulfonated OMC catalyst. The total monosaccharide yield of 43.4% was achieved when the catalyst was used to catalyze the saccharification of cellulose and rice straw substrates [15]. Dong et al. prepared an OMC-based solid acid catalyst via the evaporation-induced self-assembly method using phenolic resin as a carbon precursor, F127 as a templating agent, and sulfuric acid as a sulfonation agent. The solid acid catalyst effectively catalyzed the condensation of phenol with acetone [16]. Given the stable nature of carbon materials, sulfonation involving concentrated sulfuric acid must be conducted at high temperatures (approximately 80–150 °C). Some researchers have applied the diazonium coupling method to functionally modify the surfaces of carbon materials [17, 18]. Therefore, the diazonium coupling method can also be used to sulfonate carbon materials.

Waste cooking oils are considered as waste and resources and should be harmlessly treated and utilized. China produces more than 30 million tons of waste oil each year [19]. Waste cooking oils can be used to synthesize fatty acid methyl esters (FAMES) via transesterification with methanol. FAMES, in turn, can be used as raw materials for biodiesel and surfactants [20–22]. In addition, vegetable oils have been subjected to epoxidation. The products of vegetable oil epoxidation can be used as lubricant base oils [23], coatings [24], and plasticizers [25]. Waste cooking oils mainly comprise a mixture of various fatty acid triglycerides. The

transesterification of triglyceride and methanol comprises a three-step reversible series of reactions (Scheme 1a). First, triglycerides and methanol form diglycerides and FAMES. Diglycerides continue to react with methanol to form monoglycerides and FAMES. Monoglycerides continue to form glycerol and FAMES with methanol. The mechanism of acid-catalyzed transesterification is shown in Scheme 1b. The carbonyl group of the triglyceride is first protonated into a carbocation by an acid catalyst. The carbocation then forms a tetrahedral intermediate that is finally decomposed into a fatty acid methyl ester by methanol [26].

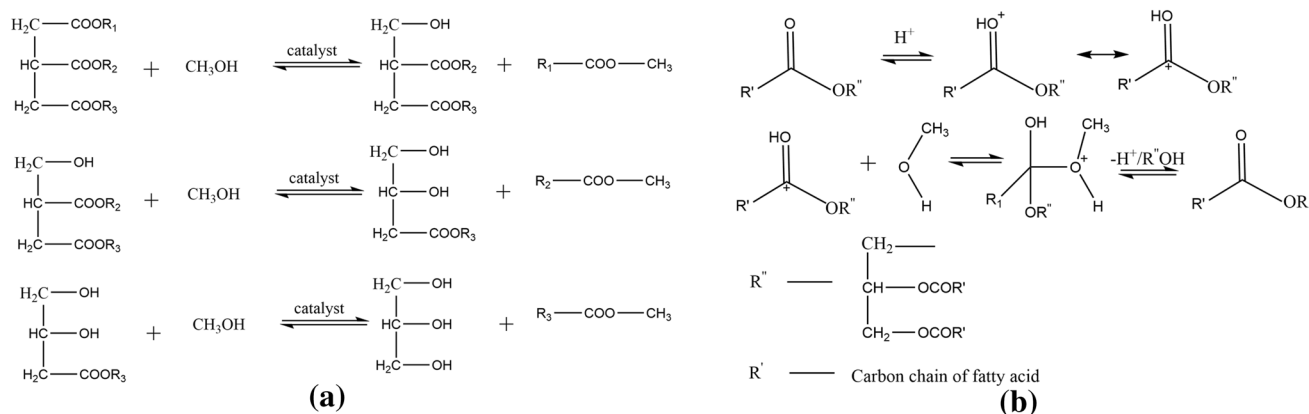
The epoxidation of triglyceride involves the formation of peroxyformic acid by formic acid and hydrogen peroxide under the action of an acid catalyst. Peroxycarboxylic acid then attacks the  $\text{C}=\text{C}$  double bond of the triglyceride to form an epoxide in situ. The reaction of peroxyacid with the  $\text{C}=\text{C}$  double bond is a cis electrophilic addition reaction wherein peroxyacid acts as an electrophile. The reaction is facilitated upon the connection of a carbon atom to an electron-donating group [27] (Scheme 2).

In this work, we prepared the ordered mesoporous molecular sieve SBA-15. We then used SBA-15 as a template to synthesize OMC materials via the inverse replication method. We obtained the solid acid catalysts, i.e., OMC-SS and OMC-DS, by sulfonating OMC materials through sulfuric acid heating and sulfanilic acid diazonium coupling, respectively. We then applied OMC-SS and OMC-DS to catalyze the transesterification and epoxidation of waste frying oil.

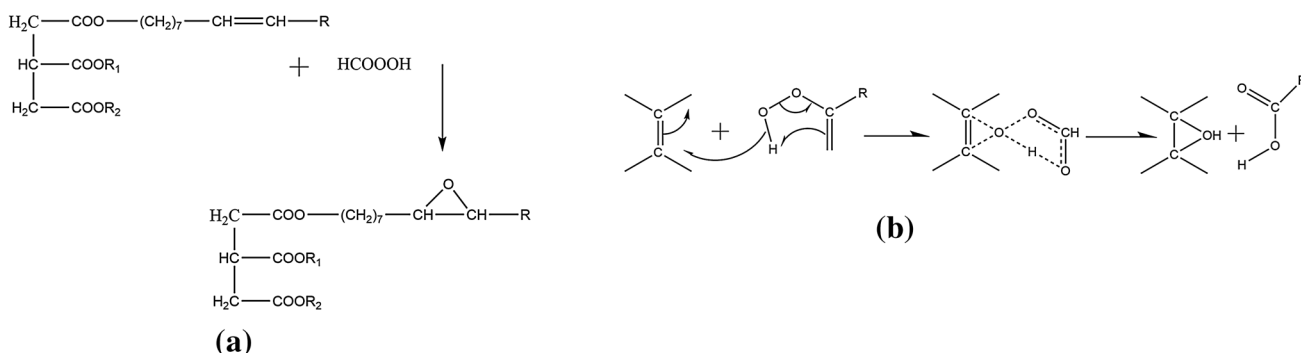
## 2 Experimental

### 2.1 Materials

P123 (PEO–PPO–PEO triblock copolymers), average  $M_n \sim 5800$ , was procured from Sigma-Aldrich. Tetraethyl



**Scheme 1** General equation (a) and mechanism (b) of acid-catalyzed triglyceride transesterification



**Scheme 2** General equation (a) and mechanism (b) of the epoxidation of triglyceride

orthosilicate (TEOS, 98%, reagent grade), sulfanilic acid (99.5%, AR), sodium nitrite (99%, AR), hydrofluoric acid (40%, AR), hypophosphorous acid (50 wt% in  $\text{H}_2\text{O}$ ), methanol (99.5%), and sodium hydroxide solution (0.1000 mol/L) were supplied by Aladdin. HPLC-grade (99.9%) acetonitrile was purchased from Fisher Scientific (USA). Sulfuric acid (98%), sucrose (99%, AR), hydrochloric acid (36%), formate (88%, AR), and sodium hydroxide (0.1000 mol/L) were purchased from Sinopharm Chemical Reagent Co., Ltd (China). Aqueous hydrogen peroxide (30%, AR) was procured from Beilian Chemical Reagent Co., Ltd (China). Waste frying oil was prepared in the laboratory.

## 2.2 Synthesis of SBA-15 [28]

First, 2 g of P123 was completely dissolved in a mixture of 60 g of hydrochloric acid solution (2 mol/L) and 15 g of deionized water at 40 °C with stirring. Then, 4.25 g of TEOS was slowly added to the mixture. The mixture was continuously stirred for 24 h. Subsequently, the product was placed at 100 °C for 48 h. SBA-15 was obtained after filtration and calcination at 550 °C (heating rate 1 °C/min) in air for 6 h.

## 2.3 Synthesis of OMC [7]

One gram of SBA-15 was added to a solution containing 1.25 g of sucrose, 0.14 g of sulfuric acid (98%), and 5 g of deionized water. The mixture was placed in an oven at 100 °C for 6 h and subsequently at 160 °C for an additional 6 h to obtain a black solid. The black solid was added to a solution containing 0.8 g of sucrose, 0.09 g of sulfuric acid (98%), and 5 g of deionized water with continuous stirring. The mixture was carbonized at 100 °C, 160 °C, and 700 °C under vacuum for 6 h. The final product was obtained after soaking in hydrofluoric acid solution (5%) for 24 h at room

temperature, washing with deionized water, filtration, and drying.

## 2.4 Synthesis of OMC-SS and OMC-DS

OMC materials and sulfuric acid (98%) were mixed at a ratio of 1:15 (g:mL). The mixture was heated at 160 °C under nitrogen atmosphere with stirring for 12 h. Subsequently, the mixture was cooled, washed with deionized water, filtered, and dried at 80 °C for 6 h. The obtained sample was designated as OMC-SS.

Two grams of sulfanilic acid and 1 g of sodium hydroxide were dissolved in 30 mL of deionized water at 37 °C to obtain a colorless solution. The colorless solution was then transferred to an ice water bath (0–5 °C). Next, 0.8 g of sodium nitrite was dissolved in the solution. The solution remained colorless after the addition of sodium nitrite. Subsequently, 10 mL of hydrochloric acid (30%) was slowly added to the colorless solution. A white precipitate was formed during the addition of hydrochloric acid. After the addition of hydrochloric acid, the solution was continuously stirred for 0.5 h. A total of 15 mL of hypophosphorous acid was mixed with the solution. Next, 0.25 g of OMC was added when the solution generated several bubbles. The solution was continuously stirred for several hours at room temperature until the termination of bubble generation. After filtration, the obtained solid was washed successively with distilled water, acetone, and ethanol twice and then dried at 80 °C for 6 h. The obtained sample was designated as OMC-DS.

## 2.5 Characterization methods

The microstructures of samples were characterized through TEM on Tecnai G2 F20 (FEI) (USA). N-adsorption experiments were performed with a Micromeritics ASAP 2020

Surface Area and Porosity Analyzer. XRD patterns were collected on a SmartLab (Rigaku) XRD with Cu K $\alpha$  radiation at 40 kV and 30 mA. X-ray photoelectron spectroscopy (XPS) was characterized on a Thermo Scientific/Escalab spectrometer equipped with Al K $\alpha$  radiation. Raman measurement was carried out on a Horiba Evolution Raman spectrometer (France). FTIR analysis was conducted with Nicolet 380 FTIR. The surface acid content of OMC materials was measured through acid–base titration. In this process, 0.1 g of OMC material was immersed in 20 mL of 0.1000 mol/L NaOH solution. The mixture was continuously stirred for 2 h under a nitrogen atmosphere. Subsequently, the OMC material was separated, and the remaining liquid was titrated with 0.1 mol/L HCl solution to a neutral pH. The surface acid content of the OMC material was obtained through calculation.

## 2.6 Transesterification reaction

Ten grams of waste frying oil, 16:1 (molar ratio of methanol/oil) methanol, and 0.4–0.8 g of catalyst were added to a 25 mL stainless steel tank reactor. The mixture was stirred at 1500 rpm. Transesterification was performed at 140–200 °C for 1.0–3.0 h. The FAME product was analyzed using a Waters 2489 liquid chromatograph (Waters Corporation, Milford, USA) equipped with a UV/visible detector (205 nm detection wavelength) and a Sunfire C18 column. The equation for FAME yield is

$$Y = m_{\text{FAME}}/m_{\text{oil}} \text{ wt}\%,$$

where  $m_{\text{FAME}}$  is the mass of FAMEs in the product and  $m_{\text{oil}}$  is the initial mass of waste frying oil.

## 2.7 Epoxidation reaction

The reaction was performed in a four-necked glass flask equipped with a condenser, dropping funnel, and mechanical stirrer. Fifty grams of waste frying oil, 4 g of formate, and 0.75–2.25 g of catalyst were added to the flask. The mixture was maintained at 20 °C. Next, 95 g of aqueous H<sub>2</sub>O<sub>2</sub> was added dropwise to the mixture within 2 h. Subsequently, the temperature was set at 20–40 °C (reaction temperature) for an additional 2–12 h (reaction time). After the reaction, the catalyst was separated through filtration, and the rest of the crude product was washed with deionized water and dried at 80 °C under vacuum to obtain the epoxidation oil. The iodine value of the epoxidation oil was analyzed through the Wijs method in accordance with GBT5532-2008. The epoxy value was obtained through the hydrochloric acid–acetone method in accordance with GBT1678-2008.

The double-bond conversion rate  $X$  and relative epoxy yield  $Y$  can be calculated using Eqs. (1 and 2), respectively

$$X = [(IN_0 - IN)/IN_0] \times 100 \quad (1)$$

$$Y = (EO_{\text{exp}}/EO_{\text{th}}) \times 100 \quad (2)$$

$$EO_{\text{th}} = \{IN_0/2A_I/[100 + (IN_0/2A_I) \times A_O]\} \times A_O \times 100 \quad (3)$$

$IN_0 = 126 \text{ g}/100 \text{ g}$ , initial iodine number;  $EO_{\text{th}} = 7.36 \text{ mol}/100 \text{ g}$  is the theoretical epoxy oxygen number. It can be calculated using Eq. (3)  $A_I$  and  $A_O$  are the relative atomic weights of the iodine and oxygen atoms, respectively [29].

## 3 Results and discussion

### 3.1 TEM

The TEM and SEM images of SBA-15, OMC, OMC-SS and OMC-DS are presented in Fig. 1. The ordered mesoporous channels of SBA-15 are visible in Fig. 1a. The mesoporous channels in SBA-15 are connected by micropores in the walls of the main channels [7]. Given that OMC formed via the reverse replication of SBA-15 [7], carbon nanorods in OMC were interconnected by slender carbon rods that had formed in micropore channels. The retention of the original ordered mesoporous structures by sulfonated OMC (Fig. 1c, d) indicates that pore structure was not drastically influenced by sulfonation. The SEM image of SBA-15 is presented in Fig. 1e. The figure shows that SBA-15 has a rod-like structure with diameters of 400–600 nm. OMC is an inverse replica of SBA-15. Correspondingly, the shape and size of OMC were similar to those of SBA-15 as shown in the SEM image in Fig. 1f. The shapes and sizes of OMC-SS and OMC-DS remained essentially unchanged after sulfonation (Fig. 1g, h).

### 3.2 N<sub>2</sub>-BET

Figure 2 shows the pore diameter distributions and N<sub>2</sub> adsorption–desorption isotherms of the materials. The density functional theory (DFT) method was used to calculate the pore diameter distributions of the materials from the adsorption branches of the isotherms. Figure 2a shows that SBA-15 had a typical IV-type N<sub>2</sub> adsorption–desorption isotherm with a H1-type hysteresis loop that is representative of the presence of mesopores. SBA-15 exhibited a narrow and unimodal pore diameter distribution and an average pore diameter of 5.5 nm (Table 1). OMC, OMC-SS, and OMC-DS had typical IV-type N<sub>2</sub> adsorption–desorption isotherms with H4-type hysteresis loops that are indicative of small pore sizes. As presented in Table 1, the average pore diameters of OMC, OMC-SS, and OMC-DS fell in the range of 3.0–3.3 nm and were less than those of SBA-15. The mesopore diameters of these materials no

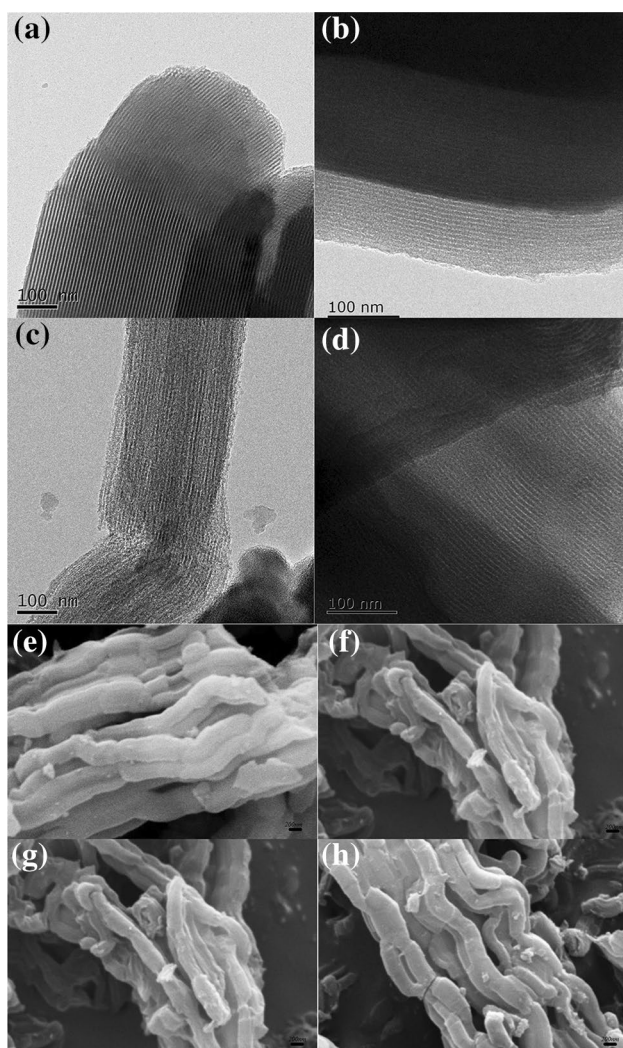


**Fig. 1** TEM and SEM images of **a, e** SBA-15; **b, f** OMC; **c, g** OMC-SS; and **d, h** OMC-DS

longer exhibited a unimodal distribution. Instead, similar to those of the materials reported by Fang et al. [30], the mesopore diameters of these materials presented a bimodal distribution.

The specific surface areas of the samples were obtained using the Brunauer–Emmet–Teller (BET) model. The BET surface area of SBA-15 was 1066 m<sup>2</sup>/g (Table 1), whereas that of OMC had increased to 1,144 m<sup>2</sup>/g. Węgrzyniak et al. prepared SBA-15 and mesoporous carbon with surface areas of 756 and 1411 m<sup>2</sup>/g, respectively [31]. Juárez et al. synthesized Ti-SBA-15 and mesoporous carbon with surface areas of 1020 and 1044 m<sup>2</sup>/g, respectively [32]. The surface areas of OMC decreased from 1144 to 924 m<sup>2</sup>/g (OMC-SS) and 1001 m<sup>2</sup>/g (OMC-DS) after sulfonation. This reduction may be attributed to the removal of free carbons in the pores of OMC after sulfonation.

### 3.3 XRD

The small-angle XRD patterns of SBA-15, OMC, OMC-SS, and OMC-DS are shown in Fig. 3. The XRD pattern of SBA-15 showed a strong diffraction peak and two weak peaks that can be assigned to the (100), (110), and (200) planes of a 2D hexagonal structure (p6 mm). The presence of these peaks shows that SBA-15 possessed a well-ordered porous structure. The XRD pattern of OMC continued to exhibit one strong diffraction peak that can be indexed to the (100) plane. This result indicates that mesoporous carbon presented an ordered porous structure that is an inverse replica of the structure of SBA-15 [33]. However, the (100) plane peaks in the XRD spectra of SBA-15 had drastically shifted relative to those in the XRD spectra of OMC, OMC-SS, and OMC-DS given that the structures of the OMC materials obtained through the reverse replication of SBA-15 were different from those of SBA-15. In addition, the XRD peak position is related to unit cell size, and inconsistencies in unit cell size result in peak shifts. Cheng et al. used SBA-15 as a template to fabricate mesoporous carbon through reverse-phase replication. They reported that the (100) plane peaks in the XRD spectra of mesoporous carbon materials had shifted relative to those in the XRD spectra of SBA-15 [34]. The presence of a weak diffraction peak ascribable to the (100) plane in the spectra of OMC-SS and OMC-DS implies that these materials had become poorly ordered after sulfonation. Peng et al. prepared mesoporous carbon using SBA-15 as a template. They then sulfonated the material using concentrated sulfuric acid (98%). Although TEM microscopy showed that the sulfonated mesoporous carbon (S-OMC) retained its ordered structure after sulfonation, the (100) plane peak in the XRD spectra of the material had weakened [35]. Dong et al. prepared ordered FDU mesoporous carbon. They then sulfonated the material with concentrated sulfuric acid (98%). TEM analysis showed that the sulfonated material possessed an ordered mesoporous structure. However, the (100) peak in the XRD pattern of the material had weakened. That is, XRD analysis indicated that the material became poorly ordered after sulfonation. Dong et al. explained that sulfonation may have partially destroyed the mesostructural order of the material [36]. In our work, TEM analysis implied that the ordered mesoporous structures of the carbon materials did not drastically change before and after sulfonation. However, XRD analysis showed that the intensity of the (100) plane peak of sulfonated carbon material had weakened. This result indicates that the OMC was corroded through sulfonation.

### 3.4 XPS and Raman

The C1s peak of the XPS spectrum (Fig. 4a) shows a main peak at 284.5 eV attributable to C=C (sp<sup>2</sup>) and

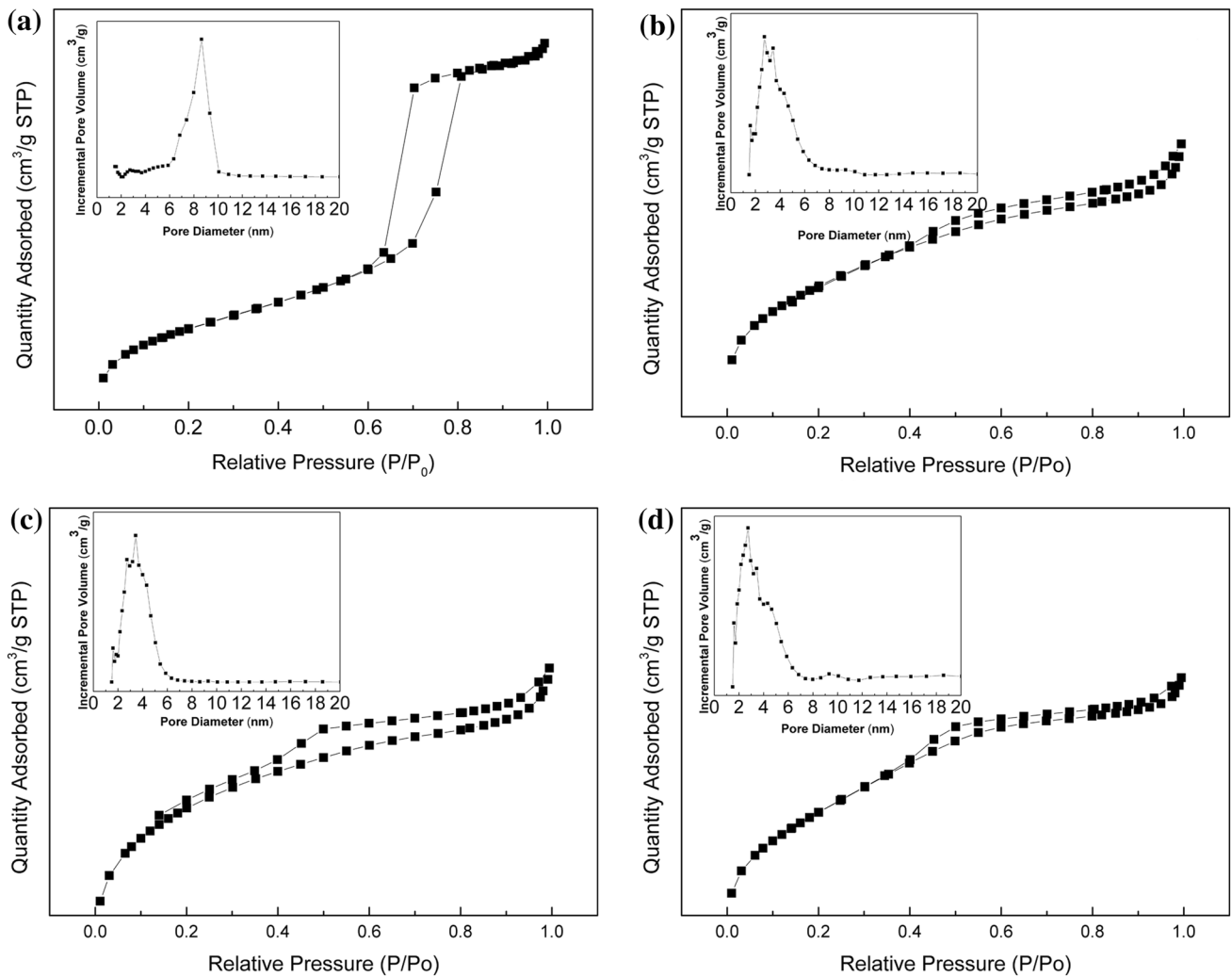


**Fig. 2** Pore diameter distribution and N<sub>2</sub> adsorption–desorption isotherms of **a** SBA-15; **b** OMC; **c** OMC-SS; and **d** OMC-DS

**Table 1** BET surface areas, average pore diameters, and surface acid content of samples

	$S_{\text{BET}}$ (m <sup>2</sup> /g)	Average pore diameter (nm)	SO <sub>3</sub> H density (mmol/g)
SBA-15	1066	5.5	–
OMC	1144	3.3	2.8
OMC-SS	924	3.0	4.0
OMC-DS	1001	3.3	3.9

C–C (sp<sup>3</sup>) bonds and the disordered graphite structure [37]. The peaks at 286.0 and 288.6 eV were ascribed to C–OH and C=O bonds, and the  $\pi$ – $\pi^*$  transition peak at 290.7 eV is typical of carbonaceous materials with nanoporous polyaromatic surfaces [38]. The Raman spectrum of mesoporous carbon material (Fig. 4b) shows two diffraction peaks at 1344 and 1582 cm<sup>−1</sup>. These peaks originated

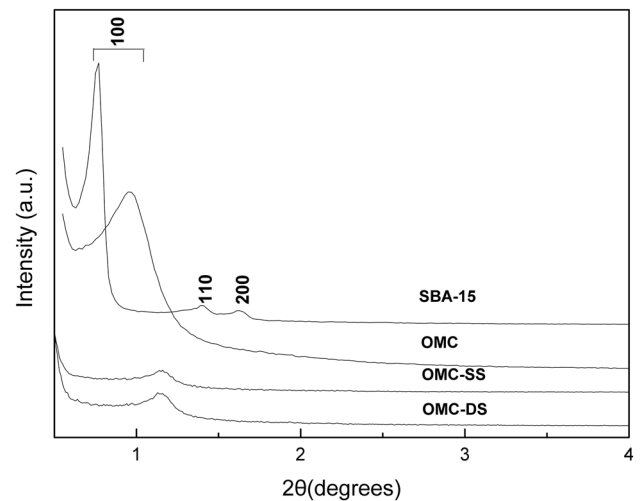


**Fig. 3** Small-angle XRD patterns of samples

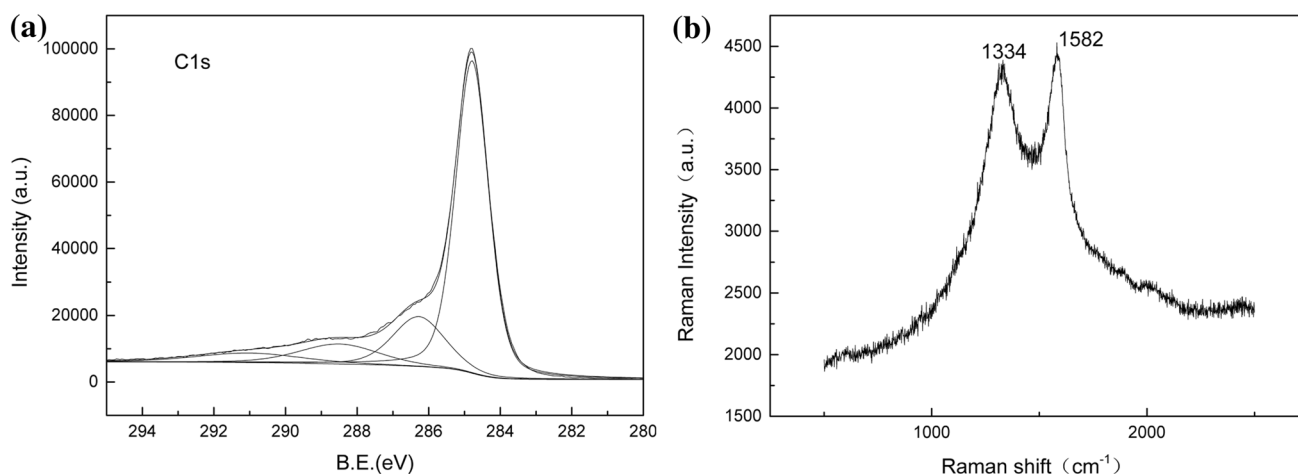


**Fig. 4** XPS C 1s spectra (a) and Raman spectra (b) of OMC

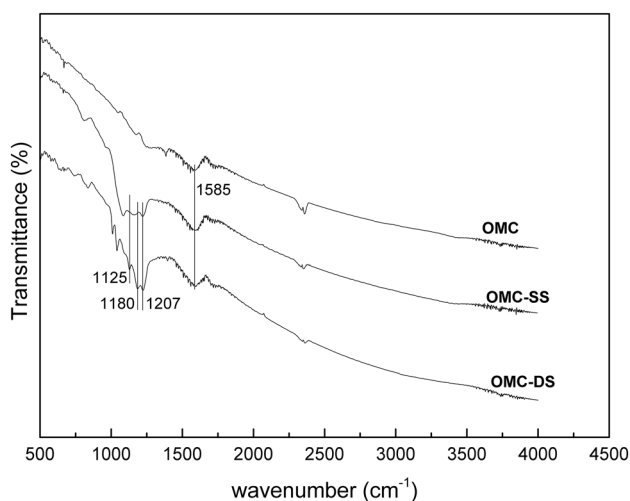


**Fig. 5** FTIR spectra of samples

from the vibration of the C–C bonds in the disordered carbon structure [39, 40]. The peak at  $1582\text{ cm}^{-1}$  was attributed to the G band, which corresponds to the  $E_{2g}$  mode of graphite and is related to the C=C vibration in the hexagonal lattice [41, 42].

### 3.5 FTIR

The peaks at  $1207$  and  $1125\text{ cm}^{-1}$  could be assigned to the stretching modes of  $\text{SO}_3\text{H}$  groups [43, 44]. The peaks at  $1180\text{ cm}^{-1}$  (stretching vibration) were consistent with  $\text{SO}_3\text{H}$  groups [45]. The peaks at  $1585\text{ cm}^{-1}$  were assigned to the stretching of the (C=C) ring [46] (Fig. 5).

### 3.6 Surface acid content

The surface acid content of OMC was  $2.8\text{ mmol H}^+/\text{g}$  and was mainly contributed by hydroxyl and carboxyl groups. The surface acid contents of OMC-SS and OMC-DS fell in the range of  $1.1$ – $1.2\text{ mmol H}^+/\text{g}$  and were contributed by sulfonic acid groups.

### 3.7 Catalytic performance in transesterification

Figure 6a shows the effect of reaction temperature on the yield of FAMES. Error bars in the figure represent standard deviations (SDs). Reaction temperature drastically affected the yield of the reaction catalyzed by OMC-SS. Yields could reach  $90.3 \pm 3.3\%$  within 3 h if transesterification was conducted at  $200\text{ }^\circ\text{C}$ . However, yields only reached  $81.8 \pm 1.6\%$ ,  $72.4 \pm 2.9\%$ , and  $26.8 \pm 0.9\%$  when the reaction was performed at  $180\text{ }^\circ\text{C}$ ,  $160\text{ }^\circ\text{C}$ , and  $140\text{ }^\circ\text{C}$ , respectively. The reaction catalyzed by OMC-DS could provide yields of up to  $89.0 \pm 2.1\%$  within 3 h when it was performed at  $200\text{ }^\circ\text{C}$  and  $180\text{ }^\circ\text{C}$  but only provided yields of  $73.1 \pm 2.2\%$  and  $56.7 \pm 1.8\%$  when it was performed at  $160\text{ }^\circ\text{C}$  and  $140\text{ }^\circ\text{C}$ , respectively. Gao et al. synthesized OMCs with hexagonal structure using phenolic resin and the surfactant F127 in ethanol through synergistic self-assembly. They then obtained S-OMCs through sulfonation with 4-aminobenzenesulfonic acid. A conversion rate close to 100% was obtained when the S-OMCs were applied to catalyze the esterification of oleic acid and methanol at  $120\text{ }^\circ\text{C}$  for 12 h [47]. Björk et al. utilized resorcinol and ordered mesoporous silica SBA-15 as raw materials and concentrated sulfuric acid as a sulfonation agent to prepare a silica/carbon complex solid acid catalyst for the transesterification of sunflower oil. The conversion rate of sunflower oil reached 85% at

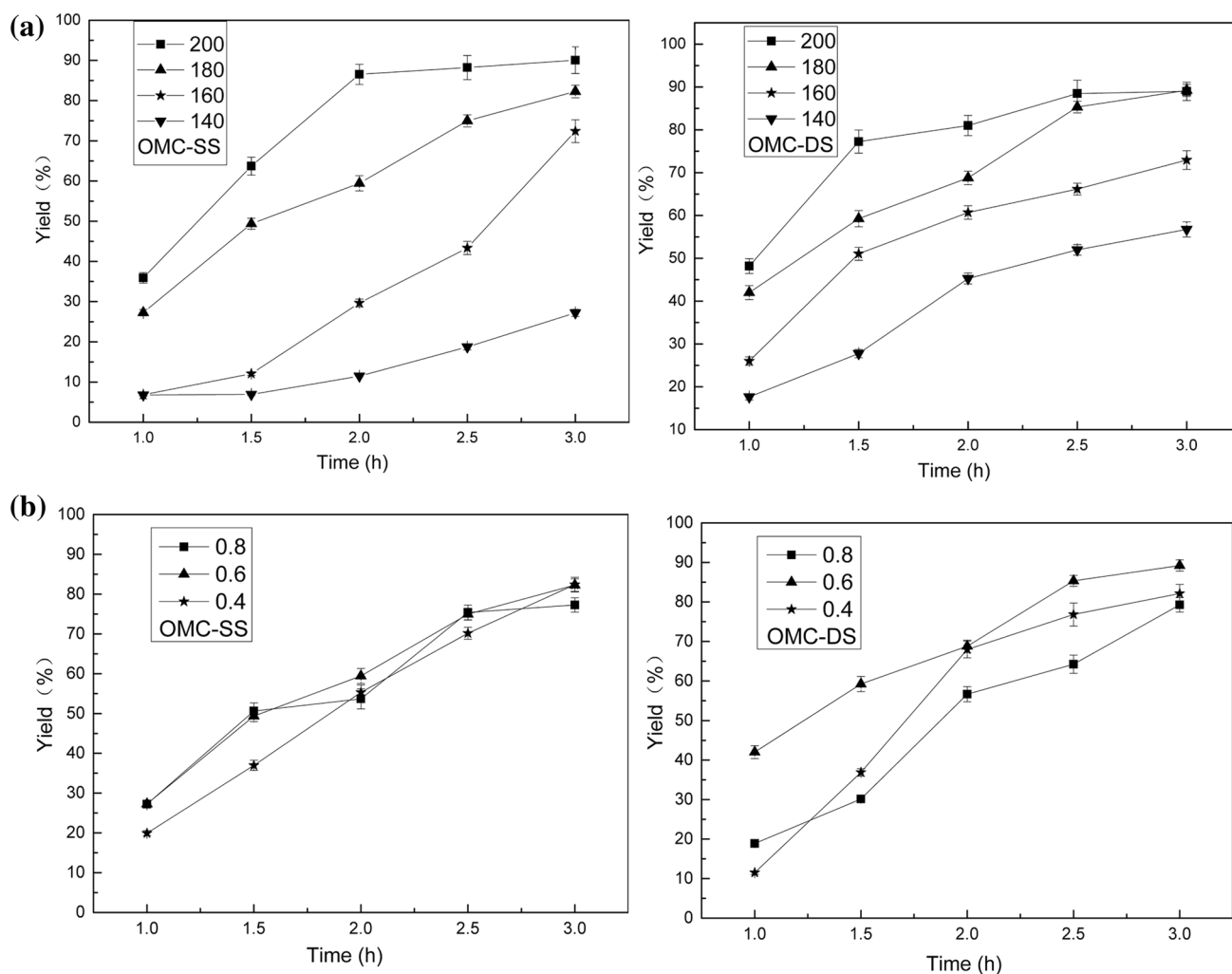


**Fig. 6** Effect of reaction temperature and catalyst amount. **a** Catalyst amount: 0.6 g; **b** reaction temperature: 180 °C

90 °C when allowed to proceed for 8 h [48]. Shah et al. prepared a silica sulfuric acid (SSA) solid acid catalyst using silica gel as a silicon source and chlorosulfonic acid as a sulfonating agent. They reported a yield of 97% when they used the SSA to catalyze the transesterification of cottonseed oil with methanol at 100 °C for 8 h [49]. Patel et al. prepared a transesterification catalyst by supporting a silicotungstate on the ordered mesoporous molecular sieve MCM-41. They acquired a conversion rate of 81% when they used the catalyst in the transesterification of oleic acid with methanol at 65 °C for 16 h [50]. Karimi et al. prepared water-tolerant sulfonic acid-based periodic mesoporous organosilicas (PMOs). They obtained a yield of 78% when they applied the PMOs to catalyze the transesterification of rapeseed oil and methanol at 150 °C for 4 h [51]. Low-temperature (65 °C–150 °C) transesterification or esterification provided good yields but required long reaction times (4–16 h). Carvalho et al. applied a

$\text{H}_3\text{PMo}/\text{Al}_2\text{O}_3$  heterogeneous catalyst in the conversion of microbial oil to biodiesel at 200 °C for 8 h and acquired an ethyl ester yield of 97% [52]. We obtained a high product yield (97%) at a similar reaction temperature (200 °C) but a prolonged reaction time (8 h). The above analysis shows that our prepared solid acid catalysts have superior catalytic performance. Figure 6b shows the effect of catalyst amount on FAME yield. Yield exceeded 0.4 g and approached 0.8 g when the amount of OMC-DS was 0.6 g. Yield negligibly changed as the amount of OMC-SS catalyst increased from 0.4 to 0.8 g. Poor reaction results were obtained when an excessive amount of catalyst was used because mesoporous carbon has low density and increasing the amount of catalyst (volume) results in agglomeration and uneven catalyst distribution in reactants. FAME yields increased to  $90.3 \pm 3.3\%$  when transesterification was performed with the reaction temperature, reaction time, and OMC-SS catalyst amount of 200 °C, 3 h, and



**Table 2** The resultant of transesterification and epoxidation reported in literatures

Transesterification/esterification			Epoxidation		
Refer-ences	Conver-sion (%)	Yield (%)	Refer-ence	Conver-sion (%)	Selectivity (%)
[47]	100		[53]	75%	98%
[48]	85				
[49]		97			
[50]	81				
[51]		78			
[52]		97			

0.6 g, respectively. FAME yield reached  $89.0 \pm 2.1\%$  when transesterification was performed with the reaction temperature, reaction time, and OMC-DS catalyst amount of  $200\text{ }^\circ\text{C}$ , 3 h, and 0.6 g, respectively (Table 2).

### 3.8 Catalytic performance in epoxidation

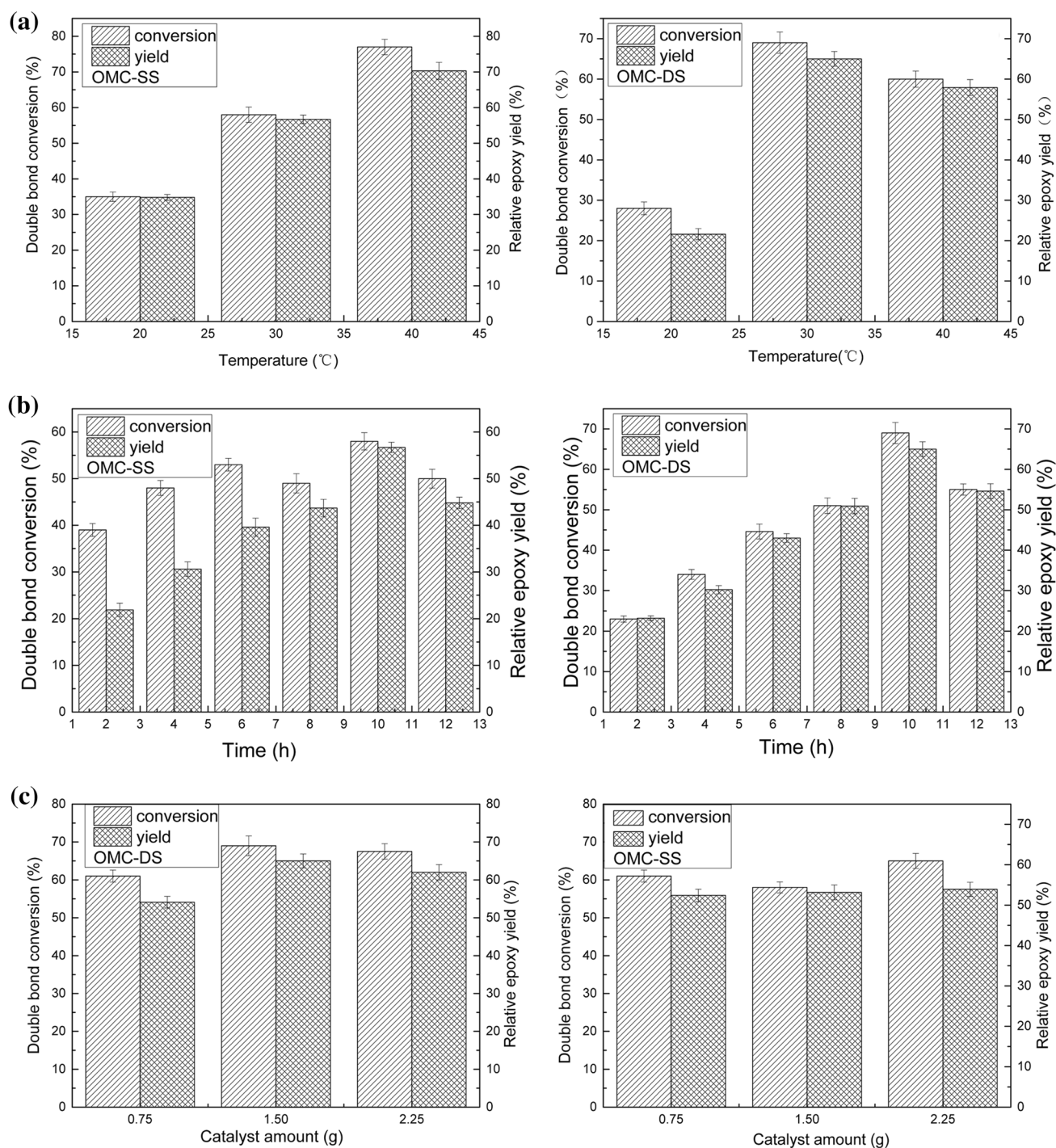
Figure 7a shows the effect of reaction temperature on double-bond conversion rates and relative epoxy yield. Error bars in the figure represent SDs. Conversion rates and yield increased when OMC-SS was used as a catalyst and the reaction temperature was increased from 20 to  $40\text{ }^\circ\text{C}$ . The maximum conversion rate of  $77.2 \pm 2.2\%$  and the yield of  $70.3 \pm 2.4\%$  were obtained when the reaction was performed at  $40\text{ }^\circ\text{C}$ . Conversion rates and yield first increased and then decreased when OMC-DS was used as a catalyst and the reaction temperature was increased. The maximum conversion rate of  $68.5 \pm 2.6\%$  with the yield of  $65.1 \pm 1.8$  was observed at  $30\text{ }^\circ\text{C}$  when OMC-DS was used as the catalyst. OMC-DS was used to catalyze the reaction of formic acid with hydrogen peroxide to form peroxyformic acid. Increasing peroxyformic acid production benefited the epoxidation of C=C bonds. The reaction results showed that high temperature favored the catalytic performance of OMC-SS.

Figure 7b shows the effect of reaction time on double-bond conversion rates and relative epoxy yield. The optimal reaction result was obtained when reaction time was 10 h and OMC-DS was used as the catalyst. The reduction in conversion rates and yield when the reaction time exceeded 10 h could be attributed to the increase in the reverse reactions of epoxidation with the decrease in the amounts of C=C and the concentration of peroxyformic acid. Figure 7c shows the effect of catalyst amount on double-bond conversion rates and relative epoxy yield. Increasing the amount of catalyst promoted the formation

of peroxyformic acid, which promoted the attack of C=C bonds by peroxyformic acid. Therefore, as the amount of catalyst increased, conversion rates substantially increased. Epoxy bond formation is more difficult than C=C bond destruction. Thus, yield did not drastically increase as the catalyst amount increased. Comprehensive consideration, the better epoxidation results were: double-bond conversion rates reached  $77.2 \pm 2.2\%$  and epoxy yield increased to  $70.3 \pm 2.4\%$  when epoxidation was performed with the reaction temperature, reaction time, and OMC-SS catalyst amount of  $40\text{ }^\circ\text{C}$ , 10 h, and 1.5 g, respectively; double-bond conversion rates reached  $68.5 \pm 2.6\%$  and epoxy yield reached  $65.1 \pm 1.8\%$  when epoxidation was performed with the reaction temperature, reaction time, and OMC-DS catalyst amounts of  $30\text{ }^\circ\text{C}$ , 10 h, and 1.5 g, respectively. Turco et al. studied the epoxidation of soybean oil with hydrogen peroxide and formic acid in the presence of an acidic ion exchange resin (Amberlyst 16) as a catalyst. A selectivity of 75% and conversion rate of 98% were observed when the reaction time was 3 h and the reaction temperature was  $55\text{ }^\circ\text{C}$  [53]. In the present work, we conducted epoxidation at low reaction temperatures ( $30\text{ }^\circ\text{C}$ – $40\text{ }^\circ\text{C}$ ) and with long durations (10 h). We obtained conversion rates (69–77%) of less than 98% but a selectivity (90–94%, selectivity = yield/conversion) of more than 75%. These results indicate that our catalyst has good selectivity.

## 4 Conclusion

We prepared OMC-SS and OMC-DS through sulfonation with sulfuric acid and sulfanilic acid, respectively. The average pore diameters of OMC-SS and OMC-DS fell in the range of 3.0–3.3 nm. OMC-SS and OMC-DS had BET surface areas of 924 and  $1001\text{ m}^2/\text{g}$ , respectively. The surface acid contents of OMC-SS and OMC-DS fell in the range of 3.9–4.0 mmol  $\text{H}^+/\text{g}$ . OMC-SS and OMC-DS were used to catalyze the transesterification and epoxidation of waste frying oil. The maximum FAME yields of transesterification reactions catalyzed by OMC-SS and OMC-DS were  $90.3 \pm 3.3\%$  and  $89.0 \pm 2.1\%$ , respectively. The conversion rates of epoxidation reactions catalyzed by OMC-SS and OMC-DS could reach  $77.2 \pm 2.2\%$  and  $68.5 \pm 2.6\%$ , respectively. The yields of epoxidation reactions catalyzed by OMC-SS and OMC-DS were  $70.3 \pm 2.4\%$  and  $65.1 \pm 1.8$ , respectively.



**Fig. 7** Effect of reaction temperature, reaction time, and catalyst amount. **a** Reaction time: 10 h; catalyst amount: 1.5 g; **b** reaction temperature: 30 °C; catalyst amount: 1.5 g; and **c** reaction temperature: 30 °C; reaction time: 10 h

**Acknowledgements** Financial support for this work from the National Natural Science Foundation of Ningxia (NZ17094), National Natural Science Foundation of China (21266001), Ningxia scientific and technological innovation leading personnel training (KJT2017006), Leading talents in technological innovation (10,000 people plan), New Catalytic Process in Clean Energy Production (ZDZX201803), Ningxia low-grade resource high value utilization and environmental

chemical integration technology innovation team project, New Catalytic Process in Clean Energy Production (ZDZX201803) are gratefully acknowledged.

## References

1. S.M.M. Ehteshami, S.H. Chan, *Sep. Sci. Technol.* **48**(10), 1459–1466 (2013)
2. J. Torres-Perez, C. Gerente, Y. Andres, *J. Environ. Sci. Health A* **47**(8), 1173–1185 (2012)
3. L. Zhou, J. Liu, X. Zhang, R. Liu, H. Huang, *Nanoscale* **6**(11), 5831–5837 (2014)
4. R.J. Carmona, L.F. Velasco, E. Laurenti, V. Maurino, C.O. Ania, *Front. Mater.* **3**, 9 (2016)
5. H. Chen, H. Wang, Z. Xue, *Int. J. Hydrogen Energy* **37**(24), 18888–18894 (2012)
6. T.N. Phan, K.G. Min, R. Thangavel, S.L. Yun, H.K. Chang, *J. Alloy Compd.* **743**, 639–645 (2018)
7. S. Jun, S.H. Joo, R. Ryoo, *J. Am. Chem. Soc.* **122**(43), 10712–10713 (2000)
8. S.H. Joo, S.J. Choi, I. Oh, J. Kwak, Z. Liu, O. Terasaki, R. Ryoo, *Nature* **412**(6843), 169–172 (2001)
9. M. Kaneda, T. Tsubakiyama, A. Carlsson, Y. Sakamoto, T. Ohsuna, O. Terasaki, S.H. Joo, R. Ryoo, *J. Phys. Chem. B* **106**(6), 1256–1266 (2002)
10. J.Y.Z. Chiou, H. Kung, C. Wang, *J. Saudi Chem. Soc.* **21**(2), 205–209 (2017)
11. C.C. Huang, Y.H. Li, Y.W. Wang, C.H. Chen, *Int. J. Hydrogen Energy* **38**(10), 3994–4002 (2013)
12. Y. Li, B. Yuan, J. Fu, S. Deng, X. Lu, *J. Colloid Interface Sci.* **408**(1), 181–190 (2013)
13. M. Regiart, J.L. Magallanes, D. Barrera, J. Villarroel-Rocha, K. Sapag, J. Rabaa, F.A. Bertolino, *Sens. Actuator B* **232**, 765–772 (2016)
14. M. Zhang, A. Sun, Y. Meng, L. Wang, H. Jiang, G. Li, *Microporous Mesoporous Mater.* **204**, 210–217 (2015)
15. E.W. Qian, L.P.P. Sukma, S. Li, A. Higashi, *Environ. Prog. Sustain.* **35**(2), 574–561 (2016)
16. X. Dong, Y. Jiang, W. Shan, M. Zhang, *RSC Adv.* **6**, 17118–17124 (2016)
17. G. Tian, J.X. Geng, Y.D. Jin, C.L. Wang, S.Q. Li, *J. Hazard. Mater.* **190**(1), 442–450 (2011)
18. J.H. Kim, T. Kim, Y.C. Jeong, K. Lee, K.T. Park, *Adv. Energy Mater.* **5**(14), 1500268 (2015)
19. Z.X. Du, Z. Tang, H.J. Wang, J. Zeng, Y. Chen, *Chin. J. Catal.* **34**(1), 101–115 (2013)
20. N.Y. Yahya, N. Ngadi, M. Jusoh, N.A.A. Halim, *Energy Convers. Manag.* **129**, 275–283 (2016)
21. I.K. Hong, H. Jeon, H. Kim, S.B. Lee, *J. Ind. Eng. Chem.* **42**, 107–112 (2016)
22. C. Wang, T.T. Shen, X.K. Wang, Y.J. Tenside, *Surfactant Deterg.* **54**(1), 64–70 (2017)
23. T. Mawatari, R. Fukuda, H. Mori, S. Mia, N. Ohno, *Tribol. Lett.* **51**(2), 273–280 (2013)
24. X.Q. Liu, Y.C. Yang, B. Gao, Y.C. Li, *J. Appl. Polym. Sci.* **133**(41), 44097 (2016)
25. G. Feng, L. Hu, Y. Ma, P. Jia, Y. Hu, M. Zhang, C. Liu, Y. Zhou, *J. Clean Prod.* **189**, 334–343 (2018)
26. L.C. Meher, D. Vidya Sagar, S.N. Naik, *Renew. Sust. Energy Rev.* **10**(3), 248–268 (2006)
27. H.B. Gao, *Organic Chemistry*, 4th edn. (Higher Education Press, Beijing, 2005), pp. 99–101
28. D. Zhao, J. Feng, Q. Huo, N. Melosh, G.H. Fredrickson, B.F. Chmelka, G.D. Stucky, *Science* **279**, 548–552 (1998)
29. S. Sinadinović-Fišer, M. Janković, O. Borota, *Chem. Eng. Process* **62**(6), 106–113 (2012)
30. L. Fang, K. Zhang, L. Chen, W.U. Peng, *Chin. J. Catal.* **34**(5), 932–941 (2013)
31. A. Węgrzyniak, S. Jarczewski, A. Wach, E. Hędrzak, P. Kuśtrowski, P. Michorczyk, *Appl. Catal. A* **508**, 1–9 (2015)
32. J.M. Juárez, B.C. Ledesma, M.G. Costa, A.R. Beltramone, O.A. Anunziata, *Microporous Mesoporous Mater.* **254**, 146–152 (2017)
33. M.J. Lázaro, L. Calvillo, E.G. Bordejé, R.R. Moliner, *Microporous Mesoporous Mater.* **103**, 158–165 (2007)
34. J. Cheng, S. Jin, R. Zhang, *Microporous Mesoporous Mat.* **212**, 137–145 (2015)
35. L. Peng, A. Philippaerts, X.X. Ke, J. Van Noyen, F. De Clippel, G. Van Tendeloo, P.A. Jacobs, B.F. Sels, *Catal. Today* **150**(1), 140–146 (2010)
36. X. Dong, Y. Jiang, W. Shan, *RSC Adv.* **6**(21), 17118–17124 (2016)
37. M. Lezanska, P. Pietrzyk, Sojka, *J. Phys. Chem. C* **114**(2), 1208–1216 (2010)
38. P. Karandikar, K.R. Patil, A. Mitra, B. Kakade, A.J. Chandwadkar, *Microporous Mesoporous Mater.* **98**, 189–199 (2007)
39. L. Rivoira, J. Juárez, H. Falcón, *Catal. Today* **282**, 123–132 (2017)
40. H. Darmstadt, C. Roy, S. Kaliaguine, *Carbon* **40**(14), 2673–2683 (2002)
41. W. Zhang, J. Cui, C.A. Tao, *Angew. Chem. Int. Ed.* **48**(32), 5864–5868 (2009)
42. B.C. Ledesma, J.M. Juárez, V.A. Valles, *Catal. Lett.* **147**(4), 1029–1039 (2017)
43. M. Zong, Z. Duan, W. Lou, T. Smith, H. Wu, *Green Chem.* **9**(5), 434–437 (2007)
44. L. Geng, Y. Wang, G. Yu, Y. Zhu, *Catal. Commun.* **13**(1), 26–30 (2011)
45. W. Li, T. Zhang, G. Pei, *Bio Resour.* **13**(1), 1425–1440 (2018)
46. A.S. Saraç, J. Springer, *Surf. Coat. Technol.* **160**(2–3), 227–238 (2002)
47. Z.H. Gao, S.K. Tang, X.I. Cui, S.J. Tian, M.H. Zhang, *Fuel* **140**, 669–676 (2015)
48. E.M. Björk, M.P. Militello, L.H. Tamborini, *Appl. Catal. A* **533**, 49–58 (2017)
49. K.A. Shah, K.C. Maheria, J.K. Parikh, *Energy Source Part A* **38**(10), 1470–1477 (2016)
50. A. Patel, N. Narkhede, *Catal. Sci. Technol.* **3**(12), 3317–3325 (2013)
51. B. Karimi, H.M. Mirzaei, A. Mobaraki, *Catal. Sci. Technol.* **2**(4), 828–834 (2012)
52. K.F. Carvalho, L.R.V. Da Conceicao, J.P.V. Silva, *Fuel* **202**, 503–511 (2017)
53. R. Turco, R. Vitiello, V. Russo, R. Tesser, E. Santacesaria, M. Di Serio, *Green Process Synth.* **2**, 427–434 (2013)

**Publisher's Note** Springer Nature remains neutral with regard to jurisdictional claims in published maps and institutional affiliations.